COBEM 2021 Florianópolis - Brasil
ABCM Associação Brasileira de Engenharia e Ciências Mecânicas
26th ABCM International Congress of Mechanical Engineering
November 22-26, 2021. Florianópolis, SC, Brazil

FLUID-STRUCTURE ANALYSIS OF PSHE HEAT EXCHANGER PLATES BY NUMERICAL APPROACH

Damylle Cristina Xavier Donati[1]
[1]Universidade Federal de Santa Catarina, Campus Joinville, R. Dona Francisca, 8300 – Bloco U, Zona Industrial Norte, Joinville – SC – Brasil.
dcxdonati@gmail.com
Rodrigo Silveira de Santiago[1]
rodrigosantiago838@gmail.com
Talita Sauter Possamai[1]
talita.possamai@ufsc.br
Renato Oba[1]
renato.oba@ufsc.br

Abstract. *Heat exchangers are widely used devices in various industries due to their operating condition's versatility in relation to temperature and pressure. In particular, in the oil and gas industry, the PSHE (Plate-Shell Heat Exchanger) model has been explored for combining the thermo-mechanical resistance of the shell-and-tube type exchangers and the compact size of the plate exchangers. Exposed to cyclic and intense thermo-mechanical loads, the model presents a need for investigation into the relationship between the flow of working fluids and the structural integrity of the device. This work addresses independent analysis in CFD and FEM as a tool of investigation for the FSI (Fluid-Structure Interaction) and aims to evaluate such interaction as to its real need in relation to hydrostatic structural analysis, as the quantitative importance of the loads generated by the flow facing the operation of the heat exchanger. Plates of Chevron angles of 45° were analyzed, in a simplified pack consisting of a pair of corrugated plates and a pair of rigid tops. Based on the evaluation of the fluid dynamic, Reynolds numbers between 1993 and 7529 were imposed as an initial condition for the flow, with an input temperature of 55 °C. Results of the fluid-structure coupling's analysis with mechanical loads resulted in high variations in the maximum value of the stress field, but not in the maximum displacement value, in relation to the hydrostatic structural evaluation for the same range of pressure input. The behavior of both variables distributions, on the other hand, shows similarity between the two methods. Still, it was found that the analysis of the mechanical load in a single way is enough for the evaluation of the phenomenon for low numbers of Reynolds. Two are the critical regions where stress peaks occur in the exchanger. The first occurs among the points of contact between the plates reaching values above the material's yield limit for loads higher than 10 bar. The tension drops dramatically - about ten times - in the region between points of contact. The second critical region occurs along the weld region, the region where there is the highest probability of failure, mainly due to the occurrence of cracks arising from the process of joining the plates. This region is located in opposite direction of the corrugations for low pressures getting to the parallel direction with the pressure increase. Normal plate displacement shows maximum values of only 5% of plate thickness, indicating system feedback between structural displacement and fluid dynamics is not required for low ranges of Reynolds number.*

Keywords: *PSHE, Fluid-Structure Interaction, CFD, FEM, Heat Exchanger.*

1. INTRODUCTION

Offshore oil extraction platforms cost, on average, 15 to 20 times more than onshore platforms, due to the high cost of drilling and prospecting tools (LIOUDIS, 2021). The high investment in machinery leads to building area rationing, increasing the cost per square meter. All devices that are not involved in the drilling and prospecting processes, in turn, must be as compact as possible. Also, Chinchane and Sumant (2021) point out that the market trend is to reduce the investment gap between on-shore and off-shore platforms, making the application more competitive.

The need for compact equipment has led to an increased demand for heat exchangers with less volume, such as plate exchangers. Such influence is due to the oil and gas industry being the fourth largest market for these devices, being just behind the chemical, refrigeration and energy production industries (GRAND VIEW RESEARCH, 2020). Yeware and Prasad (2021) estimate that PSHE-type heat exchangers will be the second largest investment in the next 5 years, second only to larger-volume heat exchangers such as shell-and-tubes, used in different applications.

Adolfsson and Rashid (2016) estimate that plate heat exchangers operate for 70% of the year, with preventive maintenance, failures or cleaning as the main causes of stoppage. It is estimated that the total cost associated with maintenance is about 32% of the total cost of operation. Plate and shell heat exchangers (PSHE) have been used and

investigated over the past decade for their versatility in size, inherited from the plates' arrangement, and the high operating limits of the shell.

As for the thermal device operation, the external flow, coming from the shells, creates both parallel and countercurrent flow patterns with the internal flow, which, in turn, flows upwards or downwards within the plate's channels.

Such behavior prevents the simplified and direct analysis coming from known correlations for general heat exchangers. For this reason, numerical analysis is preferred over other approaches, especially when dealing with more complex phenomena, which are difficult to be captured in experimental tests.

One of these phenomena is the fluid-structure interaction (FSI), which evidences the influence of the pressure, temperature and velocity fields coming from the flow in the stress and displacement state of the exchanger structure, or vice versa.

Figure 1 illustrates the scarcity of studies that encompass the analysis of fluid-structure interaction of any kind in heat exchangers. The search was made among the keywords of 706 publications in the Scopus database (from 2012 to 2022). However, among the Fatigue, Pressure Drop, CFD and Finite Element analysis subgroups, it is possible to find relevant data for the present study, in order to promote the indirect validation of the analysis.

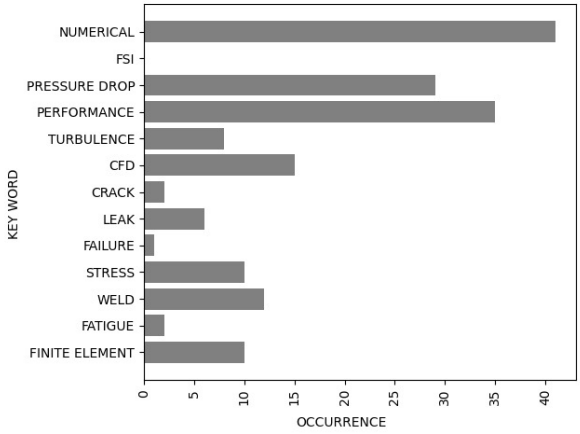

Figure 1. Occurrence of the main keywords for heat exchanger analysis.

Martins (2020) evaluated the structural behavior of PSHEs with zig-zag channels through an experimental bench, evaluating only the loading by one channel of the exchanger. Twelve stress measurements were taken along the plates, verifying that the weld regions close to the nozzles presented the higher stress. The same bench made it possible to evaluate the dynamic loading for the pack, where the fatigue life curves for different pressure loads were obtained. The same results were compared with the ASME Sec VIII Div. 2 standard, using strain gauge measurements, and it was concluded that the fatigue life reduction factor for the analyzed geometry is above the pre-established for the standard, having the ideal value between 5.9 and 6.2, well above the maximum value of 4 established by the standard. All points of failure for the experimental tests occurred in the outer weld region.

Santiago (2021, to be published) analyzed the same geometry evaluated by Martins (2020) but using a numerical approach. The simplified exchanger model, considering only 4 corrugated plates, was developed using ANSYS 18. Of the 4 plates analyzed, only two are deformable, while the others act as fixed supports only to emulate the contact points. Loading in one of the exchanger branches was applied between the central plates for the operating pressure between 8 and 16 bar. The model disregarded the material's anisotropy and plasticity effects, considering only mechanical property variations in the weld. The variation of mechanical properties in the weld did not prove to be significant when evaluating the stress state, only in fatigue analysis. Stress peaks were verified along the contact points and along the edges of the plate, some of them due to divergences between the real geometry and the numerically modeled one. Despite this, the maximum stress point found in the weld presented the same magnitude found in Martins (2020) for both simple and complex weld models and was used to perform a fatigue life comparison. In fatigue life tests, it was observed that the choice of the failure criterion and the fatigue life reduction factor has a great influence on the number of maximum cycles obtained, since the numerical model ignores many defects present in the welding process.

Beckedorff et al. (2019) employed a pair of PSHE plates with a 15° Chevron angle made of acrylic on an experimental bench in order to capture the flow displacement field via PTV. A metal device was installed around the plates to prevent separation when the flow reaches high Reynolds numbers (Re). The flow structures were evidenced, as well as velocity and pressure drop values.

Tascheck (2019) numerically analyzed three distinct configurations of Chevron angles in PSHE plates - 15°/15°, 15°/45° and 45°/45°, for nine inlet flows, including the one described in Beckedorff et al. (2019), and used water as the working fluid. The author evaluated the results of pressure drop, velocity, Nusselt number and friction factor with the help of correlations found in the literature. Furthermore, it compared the performance of two distinct turbulence models,

k-ε and SST. The SST turbulence model was more consistent with the results of Beckedorff et al. (2019), however, required more care when increasing the mesh resolution.

The present work has as objective to analyze the interaction of the internal flow with a simplified structure of 4 plates, two of them serving as movement restraint. Results comprise analyses of mechanical loads, points of maximum stress - both on the plates and on the weld - contact points and plate spacing, as well as compare data generated by uniform hydrostatic loads and by non-uniform loads from the FSI coupling on the plates of the exchanger. Thermal loads were not considered herein.

2. METHODOLOGY

The geometry used in this work is composed of four corrugated plates and a fluid domain, with their positions properly identified in Figure 2 and dimensions presented in Figure 3. The fluid domain is found inside the two central plates (2 and 3). The outer plates act as rigid supports, used to restrict the opening movement of the central plates (since the application of a pressure field inside the plates makes them behave like a pressure vessel), mimicking the rigidity of a complete pack. Plates 1 and 4, being rigid, were set to have zero displacement in all directions.

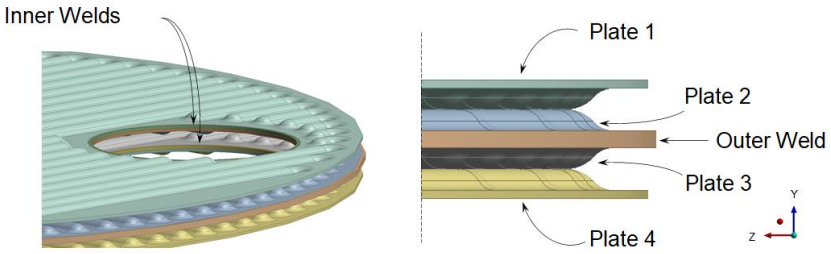

Figure 2. Arrangement of plates in modelled geometry.

PSHE has two types of fixations between plates: welding on the outer edges (between plates 2 and 3) and welding on the internal inlet and outlet nozzles (between plates 1 and 2 and plates 3 and 4). Internal flow is defined here as that delimited by the region between plates and the external weld. The external flow is defined as delimited by the plates and by the welds in the internal nozzles and comes from the flow in the PSHE shell. The welds prevent the two flows from mixing.

Extensions at the system inlet and outlet nozzles are added in the numerical model so that the flow develops fully and recirculation effects do not interfere with the flow. The extension measures are the same as defined by Tascheck (2019). Figure 4 shows the flow direction in the geometry assembly view. It also illustrates the front view of the fluid domain, showing the front view of the channel to be traversed by the flow, created by the junction of plates 2 and 3, both with a chevron angle of 45°.

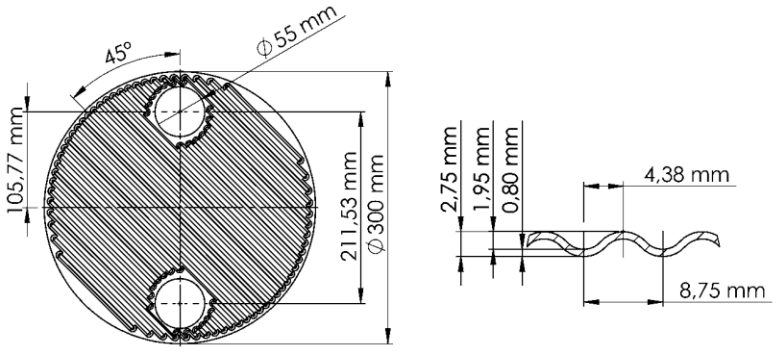

Figure 3. Dimensions of the corrugated plate a) Front view of the plate; b) Cross section of the corrugated canal.

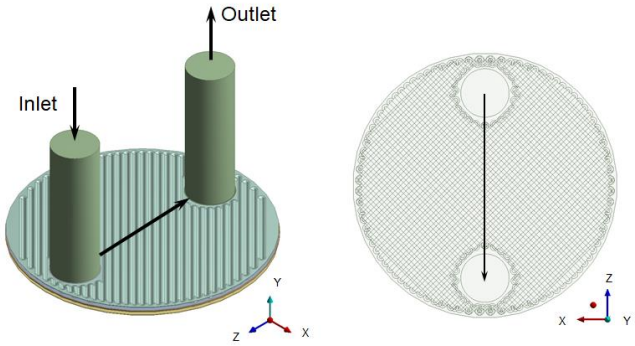

Figure 4. Flow direction and CFD model.

To obtain the pressure field, CFD analysis in the fluid domain were performed, based on the boundary conditions of Tascheck (2019): Re between 1993 and 7529 were simulated through prescribed mass flow at the inlet (Figure 4). Zero output relative pressure was set at the outlet and the no-slip condition was applied on all walls. The inlet temperature was set to 55°C as it represents the average working temperature of the heat exchanger modelled.

The finite element analysis (both hydrostatic and FSI) rely on the fixed support boundary conditions for all surfaces on plates 1 and 4, since they only function as movement restraints, and the contact conditions described in Table 1:

Table 1. Contact Conditions.

Contact Condition	**Surface**
Rough (maximum friction)	• Inferior faces of plate 1 + superior faces of plate 2; • Inferior faces of plate 2 + superior faces of plate 3; • Inferior faces of plate 3 + superior faces of plate 4.
Bonded (no separation)	• Inner welds with its respective plates; • Inner welds of plate 1with inner welds of plate 2; • Inner welds of plate 3 with inner welds of plate 4; • Outer weld with plates 2 and 3.

The difference between the two analysis (hydrostatic and FSI) lies in the applied mechanical load. In the hydrostatic analysis, the pressure is applied to the internal faces of plates 2 and 3, uniformly distributed, while in the FSI, the pressure field is caused by the flow and exported to the FEM model. Table 2 shows the mechanical properties of the material used in the plates and welds and the physical properties of the working fluid. Note that the welds and the plate use the same material (316L).

Table 2. 316L stainless steel and water properties.

Mechanical Properties – 316L (ASME Sec. II - Part D)			
Young's Module [GPa]	*Poisson's Coefficient*	*Yield Stress [MPa]*	*Ultimate Stress [MPa]*
195.00	0.31	175.00	485.00
Physical Properties – Water (55°C)			
Kinematic Viscosity [kg/ms]		*Density [kg/m³]*	
5.042×10^{-4}		985.70	

A mesh refinement analysis was developed in order to find the best mesh arrangement for numerical approach. Figures 5a and 5b show the nomenclature of the mesh regions of the solid and fluid domains, respectively. Such nomenclature serves as a guide for Table 3, which shows the specifications of the evaluated meshes. The grids were named following a AGXM standard - where A = F for fluid domain meshes and A = S for solid domain meshes; X indicates the approximate number, in millions, of elements of the respective mesh (e.g., FG5M means a fluid domain grid with 5 million elements).

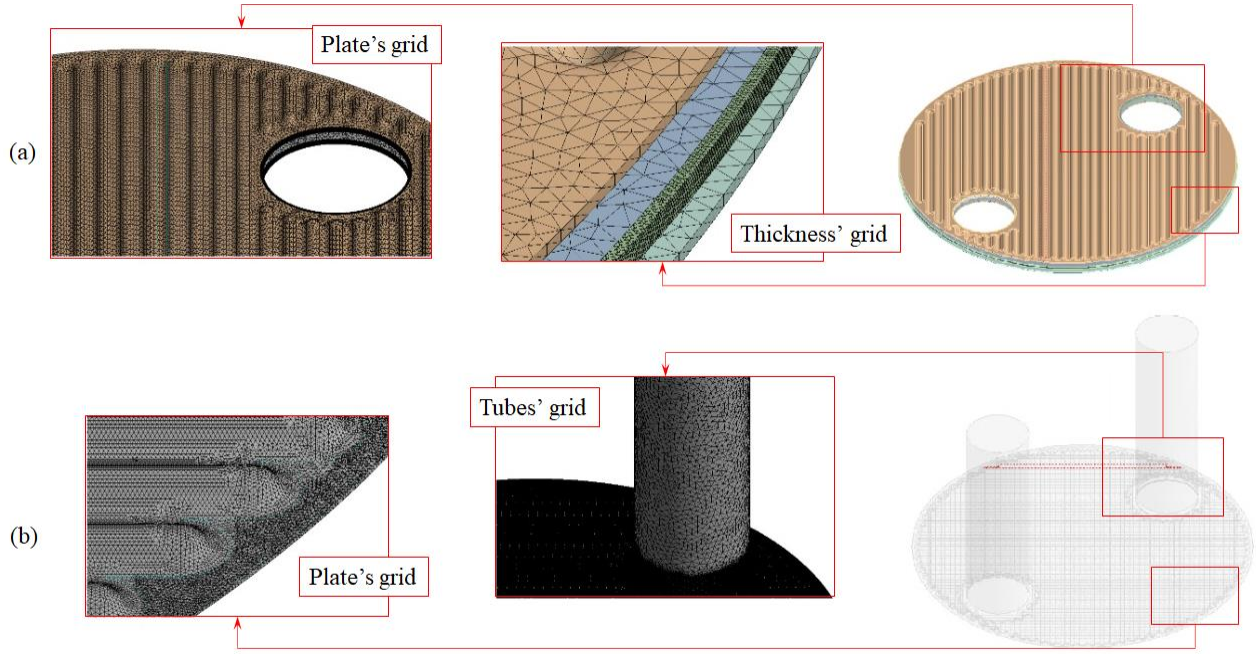

Figure 5. Details of solid (a) and fluid (b) domains' grids.

Table 3. Specifications of evaluated grids.

Fluid Domain				
Name	*Number of Elements*	*Number of Nodes*	*Tubes' grid element size*	*Plate's grid element size*
FG5M	4,766,140	7,458,504	4.0mm	0.6mm
FG12M	11,906,191	18,238,433	3.0mm	0.4mm
FG50M	49,923,218	74,613,674	2.0mm	0.2mm
Solid Domain				
Name	*Number of Elements*	*Number of Nodes*	*Thickness' grid element size*	*Plate's grid element size*
SG1.5M	1,550,113	2,993,358	0.25mm	1.5mm
SG1M	1,056,868	2,113,890	0.50mm	1.5mm

Figure 6 shows the comparative plots for the maximum von Mises equivalent stress quantities in the plate and in the weld, as well as the maximum displacement of the plate in the y-axis direction (Fig. 4). Meshes larger than 50M for the fluid domain and 1.5M for the solid domain exceeded the available computational capacity when put under FSI analysis.

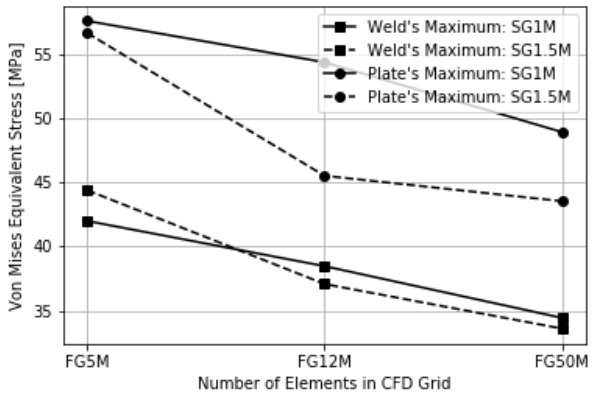

Figure 6. Mesh refinement analysis.

It is possible to notice the tendency of approximation of the results between the FG12M and FG50M meshes (approximately 10% in contrast to the 32% error between SG5M and SG50M for the weld's result) and, for this reason,

the first one was chosen for the CFD analysis in order to reduce the computational cost: the FG50M mesh resulted in an analysis time of 96h counting with CFD analysis plus FSI analysis for each estimated Reynolds number value and the FG12M mesh took about 24 hours for each Re.

The SG1.5M mesh, on the other hand, as it is the largest refinement available (added to the fact that the variation between the two meshes is only 4% for weld's maximum), was chosen for the FEM. The computer setup used in all analysis – mesh refinement and CFD, FEM and FSI analysis – was composed of an Intel® Xeon® CPU E5-2650 V4 and 128GB of RAM.

Tascheck (2019) concludes that for the 45° Chevron angle and the k-ε turbulence model, a 4 million element mesh is sufficient to achieve a 20% error in relation to the pressure drop for a pair of plates obtained by Beckedorff (2019). However, the geometry elaborated by Tascheck (2019) comprises a symmetrical fluid domain, with only half plate. Therefore, the fluid domain mesh chosen in this work of approximately 12 million tetrahedral elements with the SST turbulence model is a reasonable choice. Results were compared to Tascheck (2019) indicating 5 to 20% difference for the pressure field and velocity fields for the cases simulated herein.

Santiago (2021, to be published) performs mesh refining for the structural model (using FEM) by comparing numerical data with those obtained experimentally by Martins (2020) for a more complex corrugation geometry, reaching an optimal mesh of approximately 6 million elements. Seeking to adapt this result to the geometry covered in this work, the solid domain mesh (comprising all 4 plates) modeled to present approximately 1.5 million elements was considered sufficient, due to the simplification of the geometry and the restriction of computational power caused by the complexity of the FSI analysis.

All structural simulations, regardless of loading, were performed using FEM in the elastic regime, considering linear mechanical properties with small displacements. All CFD analysis were performed in steady state regime using the incompressible Navier Stokes equations with SST turbulence model.

The solution methodology is developed in three parts, namely:

- Hydrostatic: pressure fields were evenly distributed inside the plates. Structural integrity behavior of the system is an investigation objective through finite element method using Ansys Mechanical 18.2. Tests were performed for hydrostatic pressure loads of 0.1, 1.0, 1.5, 2.0 and 10.0 bar;
- Fluid dynamic: the numerical simulations were performed in finite volumes using Ansys CFX 18.2. The turbulence and advection models chosen were SST and hybrid, respectively. There is no heat transfer.
- FSI: the resulting flow pressure field obtained from the CFD simulation is applied to the interior of the plates as boundary conditions to the finite element method and the pressure and displacement fields compared to the hydrostatic results. Maximum stress in the weld and displacement on the Y axis (Fig. 4) are the research objectives.

3. RESULTS AND DISCUSSIONS

3.1 Hydrostatic Loading

Figure 7 shows the von Mises equivalent stress field on the external surface of plate 2. As expected, the contact points between the plates can be seen through the stress peaks along the corrugations. This behavior is more pronounced for higher loads. As observed in previous works, the contact points slightly exceeded the yield stress, only for the 10-bar loading, reaching values of 218.06 MPa for this case.

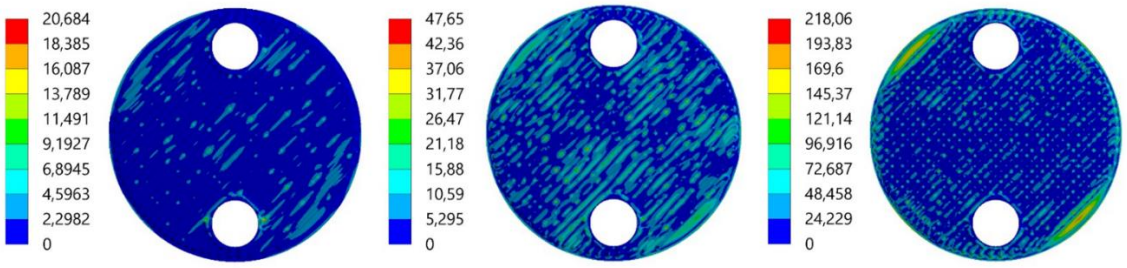

Figure 7. Von Mises equivalent stress field in MPa. Hydrostatic Pressure: 0.1 bar, 1 bar and 10 bar (left to right).

Figure 8 presents the location of the von Mises stress peaks along the weld region for the three analyzed loads. Between loads of 1 and 10 bar, one can observe the displacement of the peak stress region to coincide with the direction of the main channel. For the lowest load, the stress peak occurred in the opposite direction of the plate. This behavior occurs since the pressure is so low that the stress along the weld region is practically negligible. For the 10-bar loading, the maximum stress in the weld is 181.1 MPa, below the yield stress.

Although the level of stress found in the contact points is greater than that observed in the weld, it was observed in the literature that leakage does not occur at the contact points, despite suffering the effect of plasticity, but due to the high stresses in the weld and by the exchanger loading and unloading cycles.

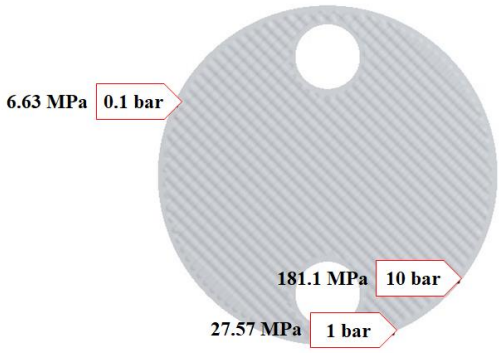

Figure 8. Equivalent stress peaks (von Mises) along the weld region for all loads.

Figure 9 presents the main results for hydrostatic loading, with the maximum von Mises equivalent stress for the weld and the plate and the average for the longest channel at first plot and the maximum displacements at the same locations. Both curves showed linear behavior, increasing with the pressure. The corrugation's average displacement is nearly zero (and for that motive, not shown at the figure) due the fact that the results for +Y and -Y contact points are overlapped since the outer plates restrict the movement of the inner plates. The maximum displacement can be found at the intersection of the plate and the weld geometries, leading the curves at Figure 9 be the same for both locations. These results will later be compared with the data obtained in the FSI tests.

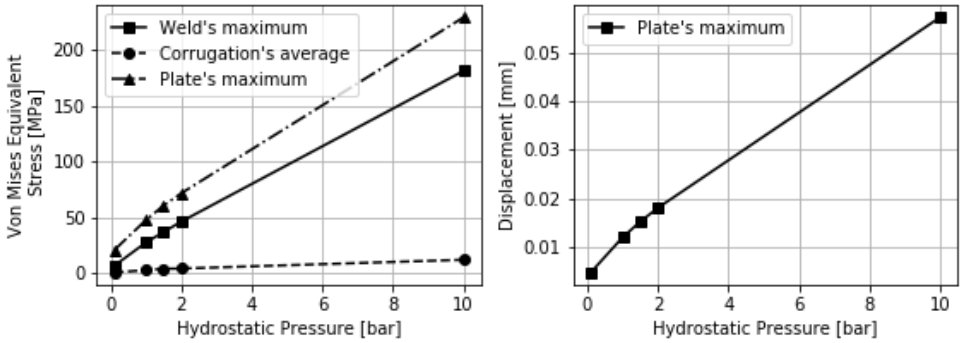

Figure 9. Hydrostatic's load maximum von Mises stress and maximum displacement in the Y direction (see Figure 4 for axis reference).

3.2 FSI

Figure 10 shows the pressure and velocity fields generated for Re = 4644. The outflow structure follows an arched pattern, being led through the channel created by the chevron angle. Upon finding the outlet, the flow generates a recirculation structure. The other Reynolds numbers studied in this work present a similar behavior, with the magnitude of the quantities varying only slightly.

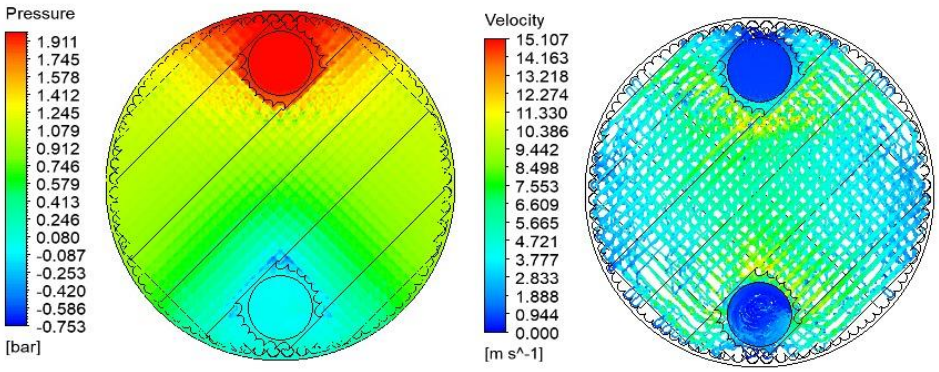

Figure 10. Pressure and velocity fields for Re = 4644 for internal flow

Figure 11 shows the stress distribution across the plates (at external surface of plate 2) for three input flows. Note the increase in the appearance of contact points as the pressure in the flow rises, from left to right. The region with the highest concentration of tension moves from the contact points to the outer weld, orthogonally to the channels' direction, as the Re rises.

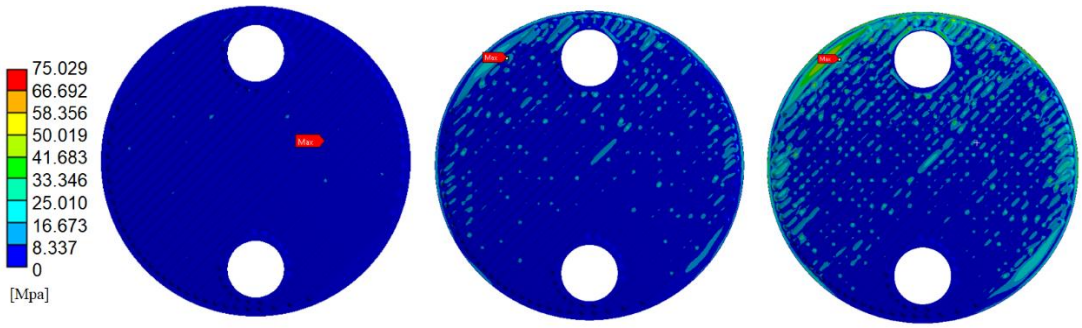

Figure 11. Von Mises' Eq. Stress Field for Re = 1993 ($\Delta P = 0.390$ bar), Re = 4644 (1.992 bar) and Re = 7529 (5.061 bar).

It is important to highlight that comparing Figures 6 and 10 the range of von Mises stress plotted are very different one from another what leads to the wrong conclusion that for uniform hydrostatic pressure more contact points between plates arise. However, the behavior and quantity of contact points for both models (hydrostatic and FSI) are similar for the average pressure of 1 bar only the range plotted in Figure 11 difficult the visualization of the contacts points.

Following the behavior observed along the plate surface, the average weld's maximum stress, indicated in Figure 12, shows significant deviation from the hydrostatical results, mostly due to the second's homogeneous load. This deviation suggests that the variable needs more investigation in further works. Plate's maximum displacement was very similar from those obtained for the hydrostatic loading, as shown in Figure 12. These results indicate that the hydrostatic simulation would not provide a good approximation for the average weld stress value, a value that is directly associated with component failure, but would for the plates' separation, associated with the flow's structure.

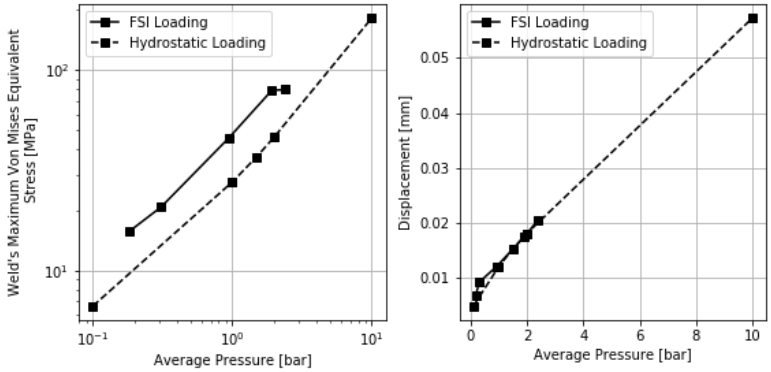

Figure 12. Comparison of maximum von Mises stress and maximum y-axis displacement values between hydrodynamic (FSI) and hydrostatic cases based on the average pressure on the plate.

Figure 13 shows the displacement's field in the perpendicular direction of the plate (in the Y axis). The magnitude of the displacement in this direction indicates the separation of the plates, since the imposed boundary conditions lead to a behavior similar to a pressure vessel. There are two areas of greater displacement in the upper section of the plate, indicating that there is higher separation in this section, just in the major pressure area. Despite the displacement peak, it can be observed that there is no great variation between the minimum and maximum values' modules, with a large portion of the plate presenting an average value. Still, the maximum displacement value represents approximately 5% of the plate thickness.

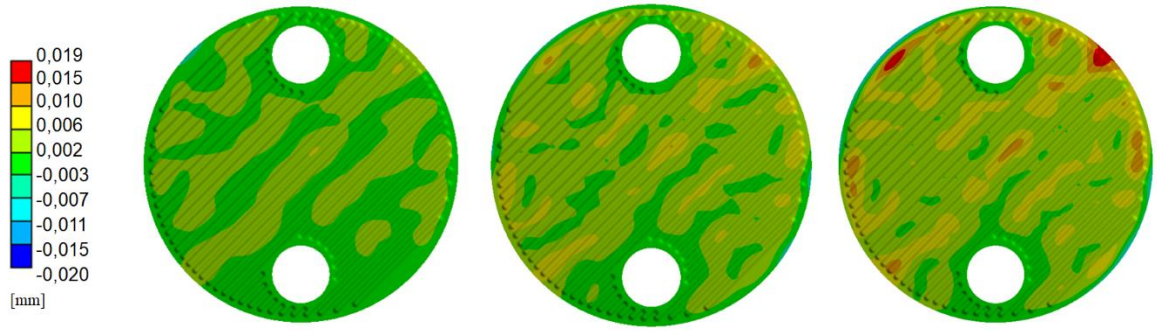

Figure 13. Displacement field in the Y direction for Re = 1993, Re = 4644 and Re = 7529, respectively

Figure 14 compiles the maximum stress data in the plate and in the weld, as well as the maximum values for the separation of the plate and the main channel (largest channel, 30 cm long). For both variables, there is a linear tendency among the applied flows, highlighting the major influence of inlet velocity both in plates' separation and maximum stress.

At the displacement's graphic, the main channel's curve shows low variation in comparison with the plate's maximum which leads to the conclusion that the stress peaks are at the plate contact points (lowest position of the corrugation).

For the points on the stress graph equivalent to the highest flows, the inversion of the curves for the plate and the weld is noted, indicating that with higher Reynolds numbers, the maximum stress values will be found mostly in the weld and no longer at the contact points.

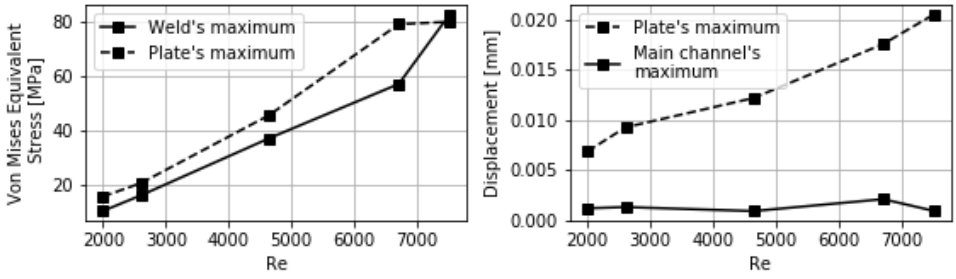

Figure 14. Maximum von Mises Equivalent stress and displacement results for hydrodynamic loading (FSI).

4. CONCLUSIONS

From the comparison between numerical modeling approaches, it is noted that for below Re = 8000, the FSI phenomenon may not be predominate in the system. Therefore, the hydrostatic approach is sufficient for the acquisition of displacements inherited to plate separation but not for the maximum stress values. Also, the variation in behavior between hydrostatic and hydrodynamic loading can be seen having a direct effect on the contact points, in the first case the contact points are obtained uniformly along the plate and in the second there is a reduction in the amount of stress peaks between inlet and outlet ports as a function of pressure drop.

As for the latter, the magnitude of normal displacements does not indicate the need for system feedback, since it represents only approximately 5% of the plate thickness. This behavior should be investigated in future works for higher loads, in which plasticity effects are observed.

It is estimated that with the increase of the Reynolds number, the stress and displacement amplitudes become accentuated, showing greater interference of the flow behavior in the integrity of the plates.

It is important to highlight that other Chevron angles configurations may behave differently and more studies involving other configurations and fatigue analysis are necessary to properly identified the effect of the FSI in this type of equipment

5. REFERENCES

Adolfsson, Marcus; Rashid, Shivan. Life Cycle Assessment and Life Cycle Cost of Heat Exchangers: A Case for Inter Terminals Sweden AB Located in Port of Gothenburg. 2016. 62 f. Master Thesis - Industrial Echology. Chalmers University of Technology, Gothenburg, 2016.

Beckedorff, L. et al., Flow Statistics in Plate and Shell Heat Exchangers Measured With PTV. International Journal of Heat and Fluid Flow. Joinville, ago. 2019.

Chinchane, Amar; Sumant, Onkar. Oilfield Equipment Market by Type (Drilling Equipment, Field Production Machinery, Pumps and Valves, and Others) and Application (On-Shore, and Off-Shore): Global Opportunity Analysis and Industry Forecast, 2019-2026. [S.l.]: Allied Market Research, 2021. Disponível em: https://www.alliedmarketresearch.com/oilfield-equipment-market-A05977. Acesso em: 05 set. 2021.

Grand View Research. Plate And Frame Heat Exchangers Market Size, Share & Trends Analysis Report by Product (Gasketed, Welded, Brazed), By Application (Chemical, HVAC & Refrigeration, Power Generation), And Segment Forecasts, 2020 - 2027. [S.l.]: Grand View Research, 2020. Disponível em: https://www.grandviewresearch.com/industry-analysis/plate-and-frame-heat-exchanger-market. Acesso em: 05 set. 2021.

Lioudis, Nick. How Do Average Costs Compare Among Various Oil Drilling Rigs?. Disponível em: https://www.investopedia.com/ask/answers/061115/how-do-average-costs-compare-different-types-oil-drilling-rigs.asp. Acesso em: 28 ago. 2021.

Martins, G. S. de M. Análise Experimental de Fadiga Mecânica em Placas de Trocadores de Calor Casco e Placas. 2020. 141 f. Dissertação (Mestrado) - Curso de Pós-graduação em Engenharia e Ciências Mecânicas, Universidade Federal de Santa Catarina, Joinville, 2020.

Santiago, R. S. de. Numerical Analysis of Mechanical Fatigue in Plate and Shell Heat Exchangers. 2021. 109 f. Dissertação (Mestrado) - Curso de Programa de Pós-Graduação em Engenharia e Ciências Mecânicas, Universidade Federal de Santa Catarina, Joinville, 2021 (no prelo).

Tascheck, B. L. Numerical Analysis of Hydrodynamic Characteristics of a Plate and Shell Heat Exchanger (PSHE). 2019. 102 f. Dissertação (Mestrado) - Curso de Programa de Pós-graduação em Engenharia e Ciências Mecânicas, Universidade Federal de Santa Catarina, Joinville, 2019

Yeware, Krunal; Prasad, Eswara. Heat Exchangers Market by Type (Shell & Tube, Plate & Frame, Air-Cooled, Microchannel, and Others), End-User Industry (Chemical, Petrochemical, Oil & Gas, HVACR, Food & Beverage, Power Generation, and Others), and Material of Construction (Carbon Steel, Stainless Steel, Nickel, and Others): global opportunity analysis and industry forecast, 2019:2026. [S.L.]: Allied Market Research, 2021. Disponível em: https://www.alliedmarketresearch.com/heat-exchanger-market. Acesso em: 05 set. 2021.

6. RESPONSIBILITY NOTICE

The authors are the only responsible for the printed material included in this paper.